JOC The Journal of Organic Chemistry

Article

pubs.acs.org/joc

C-Shaped Diastereomers Containing Cofacial Thiophene-Substituted Quinoxaline Rings: Synthesis, Photophysical Properties, and X-ray Crystallography

Catherine R. DeBlase,[†] Ryan T. Finke,[†] Jonathan A. Porras,[†] Joseph M. Tanski,[‡] and Jocelyn M. Nadeau*[,†]

[†]Department of Chemistry, Biochemistry, and Physics, Marist College, 3399 North Road, Poughkeepsie, New York 12601, United States

[‡]Department of Chemistry, Vassar College, 124 Raymond Avenue, Poughkeepsie, New York 12604, United States

Supporting Information

ABSTRACT: Synthesis and characterization of two diastereomeric C-shaped molecules containing cofacial thiophene-substituted quinoxaline rings are described. A previously known bis-α-diketone was condensed with an excess of 4-bromo-1,2-diaminobenzene in the presence of zinc acetate to give a mixture of two C-shaped diastereomers with cofacial bromine-substituted quinoxaline rings. After chromatographic separation, thiophene rings were installed by a microwave-assisted Suzuki coupling reaction, resulting in highly emissive diastereomeric compounds that were studied by UV−vis, fluorescence, and NMR spectroscopy, as well as X-ray crystallography. The unique symmetry of each diastereomer was confirmed by NMR spectroscopy. NMR data indicated that the *syn* isomer has restricted rotation about the bond connecting the thiophene and quinoxaline rings, which was also observed in the solid state. The spectroscopic properties of the C-shaped diastereomers were compared to a model compound containing only a single thiophene-substituted quinoxaline ring. Ground state intramolecular $\pi-\pi$ interactions in solution were detected by NMR and UV−vis spectroscopy. Red-shifted emission bands, band broadening, and large Stokes shifts were observed, which collectively suggest excited state $\pi-\pi$ interactions that produce excimer-like emissions, as well as a remarkable positive emission solvatochromism, indicating charge-transfer character in the excited state.

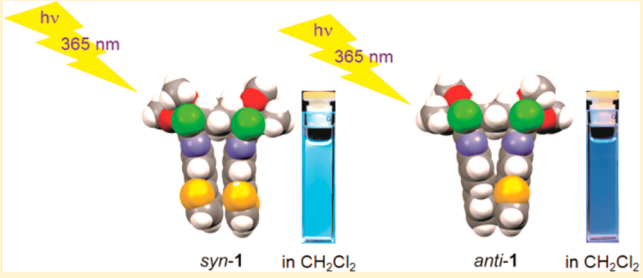

INTRODUCTION

Recently, the development of conjugated molecules with unique structural designs for studying structure−property relationships has led to a better understanding of how to manipulate organic materials for molecular electronics applications.[1−5] Creating new structures with versatile functionality and well-defined shapes is important for advancing the field of materials science because control over properties can be exercised by making deliberate structural changes. Several groups have reported the synthesis of C-shaped molecules that feature a rigid or semirigid hydrocarbon framework that holds two cofacially oriented aromatic rings at a fixed distance.[6−15] In particular, the work of Chou and co-workers on symmetrical molecules containing *syn*-facial functionalized quinoxaline rings[6] inspired us to design and synthesize *syn*- and *anti*-**1**, diastereomers whose structures are interesting by virtue of the relative positioning of the pendent thiophene rings (Figure 1).

Diastereomeric *syn*- and *anti*-**1** are structurally similar in that they both contain two cofacial thiophene-substituted quinoxaline rings that are suspended from aliphatic scaffolding. However, the subtle but major difference between them is that in *syn*-**1** the appended thiophene rings are oriented in the same direction, resulting in their potential for orbital overlap, whereas in *anti*-**1**, the thiophene rings are oriented in opposite directions with no orbital overlap possible and therefore less $\pi-\pi$ contact between the aromatic side arms. The unique topology of these diastereomers facilitates strong $\pi-\pi$ interactions between the cofacially stacked aromatic rings, which are of particular interest because these close contacts are expected to provide an effective conduit for electron transport in molecular electronics applications.[16−19] Recently, much attention has been paid to the design of small molecules and polymers specifically for probing the optoelectronic properties of π-stacked systems.[20−28]

Previous synthetic work on related molecules[6] focused on structures with symmetrical aromatic side arms. By design, we set out to explore the generation of structures with unsymmetrical side arms leading to a diastereomeric pair. Synthesis of *syn*- and *anti*-**1** was completed in four steps, of which the first three steps were adapted from Chou and co-workers,[6] including an inverse-demand Diels−Alder reaction, a ruthenium-catalyzed oxidation, a condensation, and a Suzuki coupling reaction. Model compound **2** was synthesized as a reference

Received: January 9, 2014
Published: April 28, 2014

dx.doi.org/10.1021/jo500053m | J. Org. Chem. 2014, 79, 4312−4321

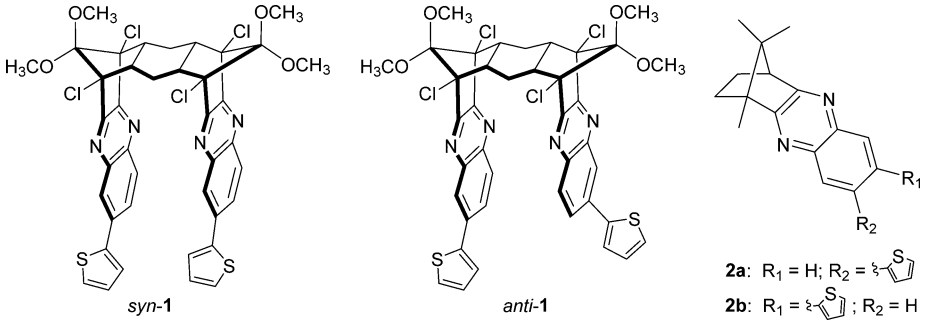

Figure 1. Structures of C-shaped molecules *syn*- and *anti*-**1** and model compound **2**.

Scheme 1. Synthesis of *syn*- and *anti*-1[a]

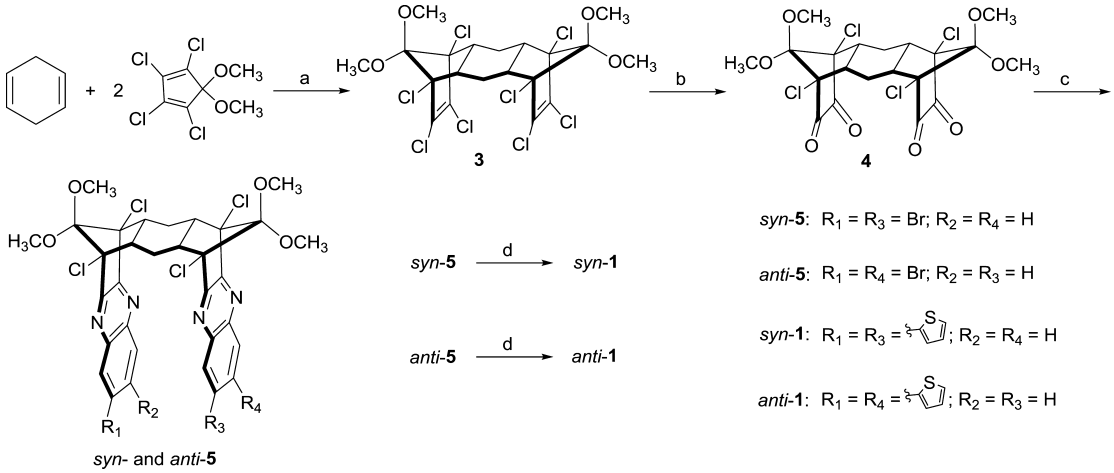

[a]Reagents and conditions: (a) *p*-xylene, MW 200 °C, 30 min; (b) $RuCl_3·3H_2O$, $NaIO_4$, $CHCl_3$/MeCN, 0 °C, 69 h; (c) excess 4-bromo-1,2-diaminobenzene, $Zn(OAc)_2$, chlorobenzene, MW 200 °C, 30 min; (d) $Pd(PPh_3)_4$, Na_2CO_3, 2-thienylboronic acid, toluene, EtOH, MW 120 °C, 30 min.

compound by related methods to explore the photophysical properties of the thiophene-substituted quinoxaline ring, a chromophore combination for which little photophysical information is known.[29−32] Herein, we present the synthesis and characterization of these structurally interesting compounds, including X-ray crystallographic analysis and comparison of the UV−vis absorption and fluorescence emission behavior of *syn*- and *anti*-**1** to one another and to model compound **2**. Collectively, the results reveal a high yet variable degree of $\pi-\pi$ overlap in these fluorescent C-shaped diastereomers that modulates their photophysical properties, a remarkable emission solvatochromism that suggests charge-transfer character in the excited state, and a potentially interesting new molecular scaffolding for studying structure−property relationships in π-stacked aromatic systems.

RESULTS AND DISCUSSION

Synthesis. Synthesis of *syn*- and *anti*-**1** was carried out in four steps. A physical separation of the diastereomers was accomplished after the third step by a chromatographic separation of the dibromide precursors, *syn*- and *anti*-**5** (Scheme 1). The first three steps in the synthesis were modeled after the approach reported by Chou and co-workers,[6] and compounds **3**[33] and **4**[34,35] were known previously. Protocols for the synthesis of **3** and the condensation leading to *syn*- and *anti*-**5** were adapted to microwave-assisted reactions in this work.

First, 2.1 equiv of 5,5-dimethoxy-1,2,3,4-tetrachlorocyclopentadiene underwent an inverse-demand Diels−Alder reaction with 1 equivalent of 1,4-cyclohexadiene to form octachloro **3** in 70% yield with microwave heating to 200 °C for 30 min, representing a significant improvement over the reported procedure of conventional heating at 80 °C for 72 h giving **3** in 50% yield.[33] Compound **3** was subsequently oxidized to bis-α-diketone **4** in 80% yield following Chou and co-workers' previously reported procedure where the same yield was obtained.[6] Accordingly, an aqueous solution of $RuCl_3·3H_2O$ and $NaIO_4$ was added to **3** and stirred at 0 °C for 69 h in a 1:1 $CHCl_3$/MeCN mixture. Compound **4** was condensed with an excess of 4-bromo-1,2-diaminobenzene in the presence of a catalytic amount of $Zn(OAc)_2$ with microwave heating in chlorobenzene (200 °C for 30 min) to afford crude **5** as a 39:39:22 mixture of *syn*-**5**, *anti*-**5**, and half-reacted byproduct, respectively (by NMR integration). The C-shaped bis-bromide diastereomers, *syn*- and *anti*-**5**, were separated and purified by column chromatography on silica gel. Although the structural differences between these diastereomers are quite subtle, their R_f values were different enough to allow for their separation by chromatographic methods because *syn*-**5** is slightly more polar than *anti*-**5**. The isolated yields of *syn*- and *anti*-**5** were 20% and 31%, respectively. With pure samples of *syn*- and *anti*-**5** in hand, we used Suzuki coupling reactions to append thiophene rings to each quinoxaline ring. Separately, *syn*- and *anti*-**5** were subjected to microwave-assisted, Pd-catalyzed Suzuki coupling with 2-thienylboronic acid to give *syn*- and *anti*-**1**, respectively, in modest yields after purification by chromatographic methods

dx.doi.org/10.1021/jo500053m | J. Org. Chem. 2014, 79, 4312−4321

Scheme 2. Synthesis of 2.[a]

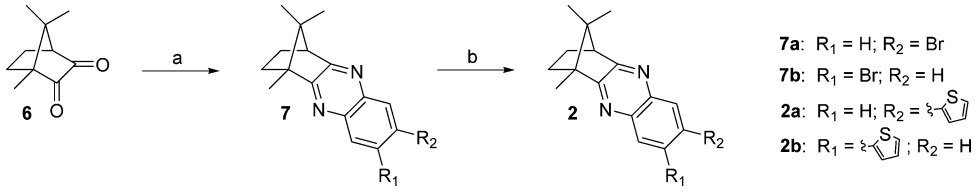

[a]Reagents and conditions: (a) 4-bromo-1,2-diaminobenzene, $CuSO_4 \cdot 5H_2O$, EtOH, rt, 100 min; (b) $Pd(PPh_3)_4$, Na_2CO_3, 2-thienylboronic acid, toluene, EtOH, MW 120 °C, 30 min.

(*syn*-**1**, 53%; *anti*-**1**, 65%). All synthetic intermediates and final products were fully characterized by ^1H and ^{13}C NMR spectroscopy, and all new compounds were also analyzed by exact mass spectrometry. Accordingly, the structures of previously reported **3** and **4** were confirmed, as our spectroscopic data matched those published in previous work.[33,34] The more salient features of the NMR spectroscopy data confirming the structures of previously unknown *syn*- and *anti*-**5** and *syn*- and *anti*-**1** are described below.

Compound **2** was synthesized following a route similar to that used to make *syn*- and *anti*-**1**, but the condensation reaction for installing the quinoxaline ring was carried out under $CuSO_4$-catalyzed conditions at room temperature (Scheme 2).[36]

(±)-Camphorquinone (**6**) was reacted with 4-bromo-1,2-diaminobenzene in the presence of 10 mol % of $CuSO_4 \cdot 5H_2O$ to give **7** in 44% yield as a 58:42 mixture of regioisomers (by NMR integration). The mixture of **7a** and **7b** was subjected to a microwave-assisted Pd-catalyzed Suzuki coupling reaction with 2-thienylboronic acid under the same conditions used to produce **5**, which yielded **2** as a mixture of regioisomers in 12% yield. Initially, the crude sample of **2** was purified by chromatography on silica gel, and the two isomers were isolated together to give **2** as a 56:44 mixture of **2a** and **2b** (by NMR integration). Additional purification of the sample was required, which was accomplished by recrystallization. The resulting sample of **2** was a mixture enriched in one of the two regioisomers (83:17), but recrystallization led to the diminished overall yield. The mixture of regioisomers was carried forward to the photophysical studies because the optical properties of **2a** and **2b** were not expected to be significantly different. Compounds **7** and **2** were fully characterized by ^1H and ^{13}C NMR spectroscopy and exact mass spectrometry. Characteristic peaks for each regioisomer were observed in the ^1H and ^{13}C NMR spectra of **7** and **2** for some of the nuclei and are reported in pairs when applicable (vide infra).

NMR Spectroscopy. The ^1H NMR spectra of *syn*- and *anti*-**5** and *syn*- and *anti*-**1** all showed evidence of the bridging cyclohexane adopting a boat conformation in solution, which is consistent with previous work on similar molecules[6] and the solid state structure (vide infra). The methylene protons attached to $C_{a/a'}$ at the center of the boat-shaped cyclohexane are each in very different shielding environments (Figure 2). The protons that point downward between the quinoxaline rings are strongly shielded such that they appear as multiplets upfield of TMS around −1 ppm in the ^1H NMR spectra. The ^1H and ^{13}C NMR spectra of *syn*-**5** and *syn*-**1** are consistent with having a σ plane of symmetry, and subsequently, those of *anti*-**5** and *anti*-**1** are consistent with having a C_2 axis of symmetry (Figure 2). The unique symmetry of the *syn* and *anti* isomers of **5** and **1** led to subtle but distinguishable differences in their

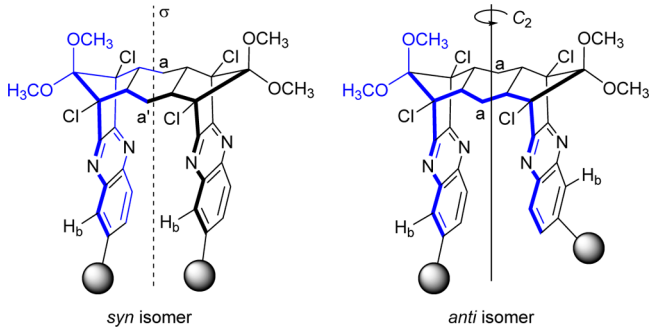

Figure 2. General structures of the C-shaped *syn* and *anti* isomers with unique proton and carbon environments outlined in blue.

NMR spectra. Most notably, in their ^{13}C NMR spectra, the *syn* isomers are predicted to have one more unique carbon environment than the *anti* isomers. Indeed, the ^{13}C NMR spectra of *syn*-**5** and *syn*-**1** showed 17 and 21 distinct carbon chemical shifts, respectively, and those of *anti*-**5** and *anti*-**1** showed 16 and 20 distinct carbon chemical shifts, respectively.

The additional carbon peak observed in the ^{13}C NMR spectra of the *syn* isomers is a result of the C_a position being two different chemical environments due to the σ plane of symmetry, giving rise to C_a and $C_{a'}$. In the *anti* isomers, the C_a position is only in one chemical environment due to the C_2 axis of symmetry. Assignment of the C_a and $C_{a'}$ peaks in the ^{13}C NMR spectra of these compounds was based on the fact that the C_a position is the most shielded and, more convincingly, on observing negative peaks for C_a and $C_{a'}$ in the DEPT 135 spectrum of *syn*-**1** (Figure S-6, Supporting Information), corresponding to the only methylene carbons. Nevertheless, the chemical environment difference between C_a and $C_{a'}$ in the *syn* isomers is subtle because the corresponding chemical shifts were unresolved at 50 MHz, but at 75 MHz there were, in fact, two corresponding C_a and $C_{a'}$ peaks for both *syn*-**5** (19.82 and 19.77 ppm) and *syn*-**1** (19.85 and 19.80 ppm).

Another notable feature of the ^1H NMR spectrum of *syn*-**1** was that it contained an unpredicted multiplet at 7.95−7.94 ppm (Figure S-5, Supporting Information) corresponding to H_b. H_b was expected to appear as a 2 Hz doublet due to meta coupling, as observed for *anti*-**1** at 7.98 ppm (Figure S-8, Supporting Information). However, expansion of the multiplet for *syn*-**1** shows two overlapping doublets with similar intensities and equivalent J values of approximately 2 Hz (Figure S-5b, Supporting Information). Moreover, the corresponding H_b proton of *syn*- and *anti*-**5** also gave rise to a single 2 Hz doublet at 7.99 and 7.94 ppm, respectively (Figures S-3 and S-4, Supporting Information). Thus, rotation about the bond through which the thiophene and quinoxaline rings are attached in *syn*-**1** appears to be restricted and, as a result, gives rise to two overlapping doublets (i.e., different

dx.doi.org/10.1021/jo500053m | J. Org. Chem. 2014, 79, 4312−4321

chemical environments of H_b), representing two different rotamers of *syn*-**1**. When the thiophene rings are cofacial, there are two possible orientations: the sulfur atoms can be adjacent to (0°, eclipsed) or opposite (180°, inverted) one another. In the ^{1}H NMR spectrum of *anti*-**1** (Figure S-8, Supporting Information), the single doublet observed for H_b at 7.98 ppm is consistent with the thiophene rings rotating freely, as would be expected because they are not proximate.

The aromatic region of the ^{1}H NMR spectra of *syn*- and *anti*-**1** was examined for evidence of ground state $\pi-\pi$ interactions between the aromatic rings in solution. Upfield shifts would be expected for the cofacially stacked quinoxaline ring protons and for some, but not all, of the thiophene ring protons in *syn*- and *anti*-**1**, depending on the isomer, compared to the corresponding protons in **2**, which contains only a single thiophene-substituted quinoxaline ring. Similar upfield shifts have been observed in other molecules with face-to-face aromatic rings.[23,24,28,37] Upfield shifts between 0.2 and 0.5 ppm for all three quinoxaline ring protons in *syn*- and *anti*-**1** (H_b, H_c, and H_d) were present compared to the corresponding protons in **2** (Table 1).

Table 1. Chemical Shifts of Thiophene-Substituted Quinoxaline Ring Protons[a]

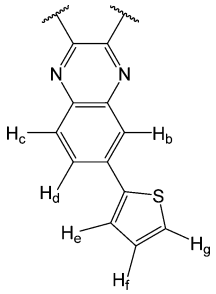

	chemical shift (ppm)		
^{1}H type	**2**	*anti*-**1**	*syn*-**1**
H_b	8.28/8.22	7.98	7.95–7.94
H_c	8.05–7.88[a]	7.64	7.76–7.65[a]
H_d	8.05–7.88[a]	7.37	7.76–7.65[a]
H_g	7.49	7.46	7.16
H_e	7.35	7.23	7.11
H_f	7.13	7.17	6.85

[a]Multiplet assigned to H_c and H_d.

H_d in *anti*-**1** showed the most significant upfield shift (>0.51 ppm), which would be expected if this proton were aimed toward the center of the thiophene ring attached to the overlapping quinoxaline ring. Upfield shifts between 0.24 and 0.33 ppm were evident for the three thiophene ring protons in *syn*-**1** (H_e, H_f, and H_g) compared to the corresponding protons in **2**, and only H_e in *anti*-**1** showed a slight upfield shift (0.12 ppm) compared H_e in **2**, which is consistent with the thiophene rings being face-to-face in *syn*-**1** but not in *anti*-**1**. The lack of upfield shift observed for thiophene protons H_f and H_g, combined with the slight upfield shift of H_e in *anti*-**1** and compared to the corresponding protons in **2**, suggests that the thiophene rings in *anti*-**1** are oriented such that the sulfur atoms face outward, away from each other and toward H_b on the attached quinoxaline ring, which was the conformation observed in the solid state (vide infra). The latter conformational preference of *anti*-**1** places H_e in the shielding zone of the other thiophene ring, whereas H_f and H_g are not. Thus, the upfield shifts observed for the quinoxaline protons of *syn*- and *anti*-**1**, the thiophene protons of *syn*-**1**, and the differently shielded thiophene protons of *anti*-**1** compared to **2** provide evidence of significant $\pi-\pi$ interactions in solution in the ground state of the C-shaped molecules.

Photophysical Properties. The photophysical properties of **2**, *anti*-**1**, and *syn*-**1** were investigated by UV–vis absorption and fluorescence spectroscopy in a range of solvents increasing in polarity from hexanes to methanol (Table 2).[38] These experiments were performed to determine the effects of molecular shape and solvent polarity on the electronic properties of the C-shaped molecules. Model compound **2** was used as a reference to compare the photophysical properties of a single thiophene-substituted quinoxaline ring to those of C-shaped *syn*- and *anti*-**1**. In addition, *syn*- and *anti*-**1** are expected to have varying degrees of cofacial overlap between the two thiophene-substituted quinoxaline rings. The UV–vis absorption spectra of **2** were relatively well-defined with two $\lambda_{max,abs}$ values ranging between 271–279 and 344–358 nm and less intense bands in between (Table 2). In contrast, *syn*- and *anti*-**1** showed two broad, structureless absorption bands with $\lambda_{max,abs}$ values ranging between 279–288 and 358–369 nm. The $\lambda_{max,abs}$ values of **2** were consistently blue-shifted by approximately 10 nm compared to the corresponding $\lambda_{max,abs}$ values of *syn*- and *anti*-**1**. Thus, the red-shifted $\lambda_{max,abs}$ values exhibited by *syn*- and *anti*-**1** compared to **2** and the fact that the absorption onsets observed for both

Table 2. Photophysical Properties of 2, *anti*-1, and *syn*-1 in Solvents of Different Polarity

	solvent	$\lambda_{max,abs}$ (nm)	$\lambda_{max,em}$ (nm)[a]	fwhm (nm)	SS (cm^{-1})[b]	Φ_F[c]
2	hexanes	271, 344	402	65	4194	–[d]
	toluene	346[e]	402	59	4026	0.01
	ethyl acetate	274, 344	406	61	4439	0.02
	chloroform	279, 352	415	63	4313	0.11
	dichloromethane	276, 345	413	62	4772	0.05
	acetonitrile	273, 344	418	66	5146	0.06
	n-butanol	277, 352	442	72	5785	0.35
	ethanol	275, 358	446	81	5511	0.37
	methanol	277, 353	451	78	6156	0.52
anti-**1**	hexanes	282, 358	412[f]	52	3661	–[d]
	toluene	362[e]	427	59	4205	0.13
	ethyl acetate	285, 362	439	64	4845	0.22
	chloroform	286, 366	441	66	4647	0.35
	dichloromethane	288, 367	445	64	4776	0.33
	acetonitrile	284, 366	461	73	5630	0.57
	methanol	288, 368	491	86	6807	0.49
syn-**1**	hexanes	279, 358	424	65	4348	–[d]
	toluene	364[e]	447	69	5101	0.20
	ethyl acetate	281, 362	459	75	5838	0.27
	chloroform	284, 368	462	75	5529	0.43
	dichloromethane	284, 369	471	78	5869	0.40
	acetonitrile	282, 366	484	92	6661	0.37
	methanol	282, 369	510	97	7492	0.21

[a]λ_{ex} = 300 nm. [b]Stokes shift, SS = $1/\lambda_{max,abs} - 1/\lambda_{max,em}$. [c]Fluorescence quantum yields were determined relative to coumarin 153 in MeOH (Φ_F = 0.45)[40] as the standard (λ_{ex} = 350 nm). [d]Not measured due to poor solubility. [e]Analyte absorption below 300 nm was obscured by solvent absorption. [f]Shoulder present at 394 nm.

dx.doi.org/10.1021/jo500053m | J. Org. Chem. 2014, 79, 4312–4321

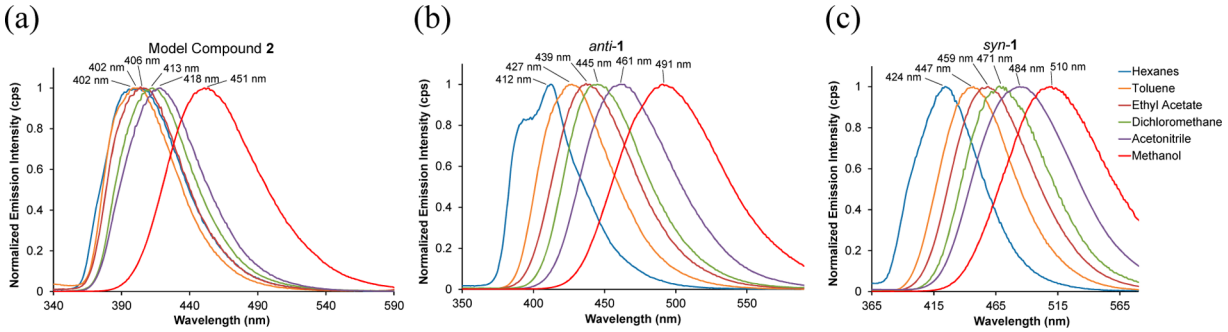

Figure 3. Normalized fluorescence emission spectra of (a) **2**, (b) *anti*-**1**, and (c) *syn*-**1** recorded in various solvents (λ_{ex} = 300 nm).

syn- and *anti*-**1** compared to **2** were always at higher intensity and longer wavelengths suggest that there are $\pi-\pi$ interactions between the cofacial aromatic rings in the ground state of *syn*- and *anti*-**1**, which were also detected by ^{1}H NMR spectroscopy.[15,37,39]

Comparison of the absorption maxima of *syn*- and *anti*-**1** to those of Chou's *syn*-bis-quinoxaline analogue without quinoxaline ring substituents reveals the effect of the thiophene ring in the thiophene-substituted quinoxaline ring chromophore.[6] Chou's analogue (Scheme 1; all R groups = H) showed two absorption maxima at 240 and 315 nm in chloroform, while the corresponding $\lambda_{max,abs}$ values for *anti*-**1** (286 and 366 nm) and *syn*-**1** (284 and 368 nm) in chloroform were red-shifted significantly by about 40−50 nm (Table 2). This comparison clearly illustrates the effect the thiophene rings have on the absorption properties of *syn*- and *anti*-**1**, namely the extended conjugation beyond the quinoxaline ring chromophore.

Fluorescence spectroscopy was performed on compounds **2**, *anti*-**1**, and *syn*-**1** in a range of solvents increasing in polarity from hexanes to methanol, and relative fluorescence quantum yields were measured[41] using coumarin 153 (Φ_F = 0.45 in MeOH)[40] as a standard (Table 2 and Figure 3). In general, **2**, *anti*-**1**, and *syn*-**1** displayed single broad, structureless emission bands in all the solvents studied. Comparisons of the emission spectra and Stokes shifts for these three compounds across any one solvent reveal a clear and consistent structure-dependent emission behavior (Table 2).

The emission bands of **2** in each solvent studied were significantly blue-shifted by 20−50 nm compared to the corresponding bands of *syn*- and *anti*-**1**, depending on the solvent. Thus, fluorescence emission from **2** appears to occur from relaxation of the single excited thiophene-substituted quinoxaline ring, or the locally excited (LE) state emission. Furthermore, in every solvent studied, the emission bands of *syn*-**1** were red-shifted by an average of 20 nm compared to those of *anti*-**1**, which is consistent with *syn*-**1** having extended orbital overlap from the cofacially arranged thiophene rings and, as such, an overall higher degree of π-stacking than *anti*-**1**. Moreover, the trend observed in the emission band position mirrored the trend in the Stokes shifts, where the Stokes shifts increased from **2** to *anti*-**1** to *syn*-**1** across every solvent studied from toluene to methanol (Table 2). As suggested by Chou and co-workers in their work on related structures, it is believed that the close proximity of the aromatic segments in *syn*- and *anti*-**1** leads to emission in these molecules from an intramolecular excimer-like state, which is consistent with the significant red-shift of the emission spectra and the large Stokes shifts observed for both *syn*- and *anti*-**1** compared to **2**.[6,15,37]

The emission properties of *syn*- and *anti*-**1** were compared to those of the *syn*-bis-quinoxaline analogue without substituents reported by Chou.[6] Chou's analogue (Scheme 1; all R groups = H) had an emission band at 395 nm in chloroform, while the emission bands of *anti*- and *syn*-**1** were at 441 and 462 nm in chloroform, respectively (Table 2). This comparison further highlights the increase in conjugation afforded by the thiophene rings and its effect on the photophysical properties of *syn*- and *anti*-**1**.

While the UV−vis absorption spectra show only a slight positive solvatochromism in the longer wavelength absorption band of compounds **2**, *anti*-**1**, and *syn*-**1**, analyzing the emission band maxima and Stokes shifts of **2**, *anti*-**1**, and *syn*-**1** as a function of solvent reveals that solvent polarity strongly affects the emission properties of these molecules, particularly the C-shaped diastereomers (Table 2). It is evident upon looking at the fluorescence emission spectra of **2** that there was no solvent-dependent emission effect present, except to a slight degree in acetonitrile and more vividly in the alcohols (Figure 3a and Table 2). Thus, in nearly all the solvents studied except the alcohols, emission in **2** is likely to occur predominantly from relaxation of the LE state. In the alcohols, the emission bands of **2** were all red-shifted from acetonitrile by more than 20 nm, and there was a slight positive solvatochromism observed within the alcohol series itself. The anomalous emission behavior of **2** in the alcohols may be due to hydrogen bonding effects or possibly to intramolecular charge-transfer (ICT) within the thiophene (donor) and quinoxaline (acceptor) unit becoming more viable in a more polar medium.[29,32,38] The full-width at half-maximum (fwhm) of the emission bands of **2** hovered around 60 nm in the solvents ranging in polarity between hexanes and acetonitrile, but then increased to 72−81 nm in the alcohols. A similar trend was evident for the Stokes shifts of **2** as a function of solvent polarity, where they were relatively small and increased steadily from hexanes to acetonitrile (from 4194 to 5146 cm^{-1}, respectively), but increased dramatically in the alcohols, reaching as high as 6156 cm^{-1} in methanol. Moreover, the quantum yields for **2** were extremely small (<0.1) in all the solvents except the alcohols, where the quantum yields increased to as high as 0.3−0.5 (Table 2). Thus, the positive solvatochromism, band broadening, higher Stokes shifts, and increased quantum yields observed for **2** in the alcohols seem to collectively suggest a significant change in the excited state structure of **2** in the polar-protic alcohols, leading to **2** becoming more emissive.[42] Perhaps there is a remarkable hydrogen bonding effect or an increase in charge-transfer character because a larger dipole moment would lead to greater excited state stabilization in a more polar medium.[43,44]

The fluorescence emission bands of both *syn*- and *anti*-**1** red-shifted and broadened dramatically, and the Stokes shifts increased as a function of increasing solvent polarity (Figure 3, panels c and b, respectively; and Table 2). The degree of the

dx.doi.org/10.1021/jo500053m | J. Org. Chem. 2014, 79, 4312−4321

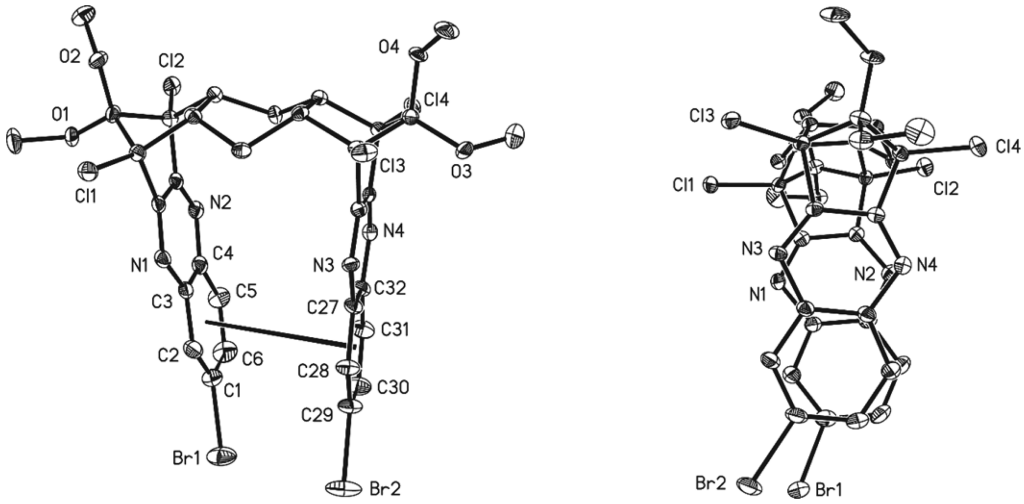

Figure 4. ORTEP diagrams (40% probability) of *syn*-**5** (crystal system, monoclinic; space group, $P2_1/c$). Hydrogen atoms are omitted for clarity. Intramolecular π-stacking centroid-to-centroid distance (shown left): 4.092(2) Å.

Table 3. Selected Transannular Metrical Parameters between the Quinoxaline Rings

	N−N distances (Å)		C−C distances (Å)		centroid-to-centroid distance (Å)[a]	centroid-to-ring plane distances (Å)[a]	ring offset distances (Å)[a]
parent molecule [ref 6][b]	4.690		3.864		4.135	4.020	0.968
syn-**5**	N1−N3	4.629(4)	C1−C29	3.917(6)	4.092(2)	3.830(3),	1.440(6),
	N2−N4	4.540(4)	C6−C30	3.885(6)		3.846(3)	1.397(6)
syn-**1**	N1−N3	4.667(5)	C9−C26	4.013(6)	4.157(3)	4.131(3),	0.462(7),
	N2−N4	4.630(5)	C14−C25	3.882(7)		4.021(4)	1.053(8)
anti-**1**	N1−N3	4.558(5)	C9−C25	3.444(6)	3.810(2)	3.778(2),	0.492(7),
	N2−N4	4.529(5)	C14−C26	3.451(6)		3.753(2)	0.659(7)

[a]Measured between the six-membered aromatic rings.[49] [b]Calculated with Mercury 3.0.[48]

observed red-shift for *syn*- and *anti*-**1** was relatively consistent from one solvent to the next, but the band broadening and Stokes shifts were significantly larger for *syn*-**1** compared to *anti*-**1** in the most polar solvents studied, acetonitrile and methanol, which in turn were much larger than the band broadening and Stokes shifts observed for **2** in these same two solvents. The fwhm values in acetonitrile were 66, 73, and 92 nm for **2**, *anti*-**1**, and *syn*-**1**, respectively, and in methanol, the fwhm varied between 78, 86, and 97 nm for **2**, *anti*-**1**, and *syn*-**1**, respectively. The more consistent positive solvatochromism and increasing Stokes shifts observed in *syn*- and *anti*-**1** across the entire solvent polarity range studied suggests stronger ICT character in the excited state of the C-shaped diastereomers compared to **2**, which could be attributed to the constrained π-orbital overlap between their cofacial quinoxaline segments, stabilizing the CT state.[45] The latter notion is further corroborated by the increased broadening and larger Stokes shifts observed for *syn*-**1** compared to *anti*-**1** because *syn*-**1** has more π-orbital overlap due to the thiophene rings being cofacial. The quantum yields of *anti*- and *syn*-**1** were fairly small in toluene and ethyl acetate (0.13−0.27), increased to moderately higher values in dichloromethane, chloroform, and acetonitrile (0.33−0.57), and then dropped slightly in methanol (Table 2). The general increase in quantum yield as solvent polarity increased for *anti*- and *syn*-**1** in the aprotic solvents suggests that there is a stabilization of the excited state by polar solvents that increases emission, perhaps a rigidification of the structure that would increase quantum yield.[42,45]

X-ray Crystallography. An X-ray diffraction study on a crystal of *syn*-**5** grown from a 20% ethyl acetate in hexanes solution led to elucidation of its solid state structure, as shown in Figure 4. A molecule of hexane that cocrystallized with *syn*-**5** is located between the quinoxaline segments of neighboring molecules (not shown).

In *syn*-**5**, the face-to-face quinoxaline rings are suspended from aliphatic scaffolding that features a boat-like cyclohexane at its center, which has also been observed in related *syn*-bis-quinoxaline structures reported by Chou and co-workers.[6] The quinoxaline rings begin to converge on one another as they extend away from the aliphatic framework, allowing for significant π-overlap between the aromatic segments. The transannular N−N distances of 4.629(4) and 4.540(4) Å and C−C distances of 3.917(6) and 3.885(6) Å in *syn*-**5** are very similar to those described for the parent *syn*-bis-quinoxaline (Scheme 1; all R groups = H), with an N−N distance of 4.690 Å and a C−C distance of 3.864 Å (Table 3).[6] Given that the bromine atoms in *syn*-**5** are both oriented toward the same side of the molecule, this leads to minor structural distortions such that the two quinoxaline rings are not perfectly equidistant nor as cofacially aligned as they are in the unsubstituted quinoxaline parent molecule.[6] In *syn*-**5**, the quinoxaline rings are twisted away from one another, presumably to alleviate steric strain

dx.doi.org/10.1021/jo500053m | J. Org. Chem. 2014, 79, 4312−4321

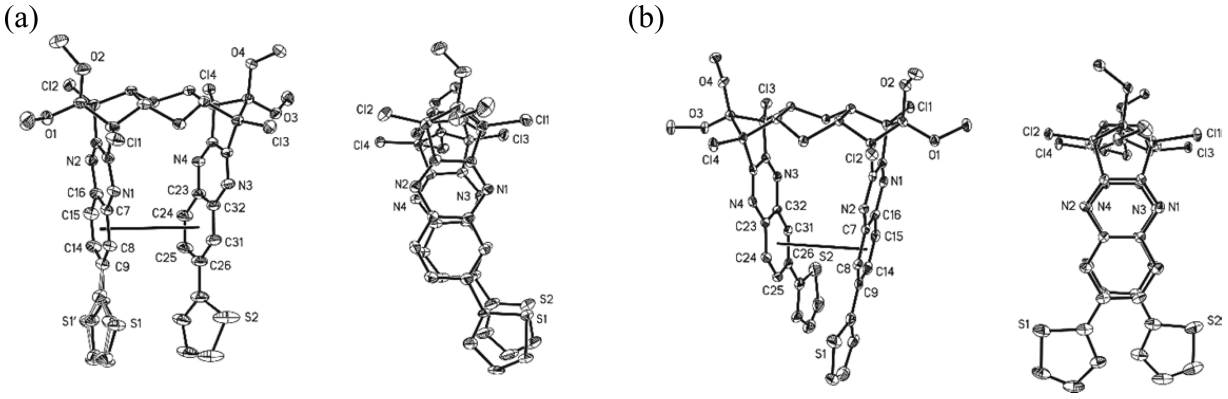

Figure 5. ORTEP diagrams (40% probability) of (a) *syn*-**1**, where the structure with thiophene ring disorder is on the left and the eclipsed rotamer is on the right (crystal system, monoclinic; space group, $P2_1/n$), and (b) *anti*-**1** (crystal system, triclinic; space group, $P\bar{1}$). Hydrogen atoms are omitted for clarity. Intramolecular π-stacking centroid-to-centroid distances (shown left): *syn*-**1** 4.157(3) Å, *anti*-**1** 3.810(2) Å.

from the intramolecular Br1−Br2 interaction at a distance of 3.7482(8) Å, which is only slightly longer than the sum of the van der Waals radii of bromine, 3.70 Å.[46] When *syn*-**5** is viewed through the quinoxaline rings, it becomes evident that the π-stacked rings are slightly slipped (Figure 4, right). In face-to-face π-stacking structures such as this, the ring centroid-to-centroid distance describes the closeness of the interaction, while comparison of the centroid-to-centroid distance and centroid-to-ring plane distances describes how slipped, or offset, the face-to-face overlap is.[47] In *syn*-**5**, the centroid-to-centroid distance of 4.092(2) Å and centroid-to-plane distances of 3.830(3) and 3.846(3) Å yield ring offset slippage parameters of 1.440(6) and 1.397(6) Å. These π-stacking parameters reflect that the quinoxaline rings in *syn*-**5** are slightly slipped in comparison to the parent compound, which exhibits a centroid-to-centroid distance of 4.135 Å, a centroid-to-plane distance of 4.020 Å, and a ring offset parameter of 0.968 Å.[48]

The X-ray structures of *syn*- and *anti*-**1** were also determined, which provide important insights into how π-stacking interactions could be influencing their photophysical properties. The molecular structures of *syn*- and *anti*-**1** are depicted in Figure 5. X-ray quality crystals of *syn*- and *anti*-**1** were grown by vapor diffusion of hexanes into $CDCl_3$ and dichloromethane, respectively. A single molecule of $CDCl_3$ cocrystallized with *syn*-**1**, whereas two molecules of CH_2Cl_2 cocrystallized with *anti*-**1** (not shown).

In the X-ray structures of both *syn*- and *anti*-**1**, the thiophene-substituted quinoxaline rings are suspended from an alkyl scaffolding that also features a boat-like cyclohexane at the center. Looking through the cleft formed between the aromatic rings, it becomes evident that the dihedral angle between the thiophene and quinoxaline rings is near zero for both *syn*- and *anti*-**1** in the solid state (Figure 5). These results are consistent with other biaryl structures like biphenyl that are known to be planar in the solid state[50] but that typically have nonzero dihedral angles on the order of 40° in the gas phase and in solution to avoid steric hindrance between the *ortho*-hydrogens when crystal packing energy benefits are not a factor.[51,52] The aromatic ring segments in both structures converge on one another as they extend away from the aliphatic spacer, as seen in *syn*-**5**, to a slightly greater degree in *anti*-**1** compared to *syn*-**1**, most likely due to steric hindrance between the *syn* substituents. However, whereas the transannular N−N distances observed for *syn*-**1** and *anti*-**1** are very similar to those observed for both *syn*-**5** and the parent *syn*-bis-quinoxaline (in the range of 4.529−4.690 Å), the transannular C−C distances of 3.444(6) and 3.451(6) Å for *anti*-**1** are significantly shorter than those observed for the other three structures, in which C−C distances are in the range of 3.864−4.013 Å (Table 3). The cofacial thiophene rings in *syn*-**1** create steric strain that is not present in *anti*-**1**, which is also consistent with the twisting of the quinoxaline rings away from one another, as noted above for *syn*-**5**. Nevertheless, the twisting of the quinoxaline rings is less pronounced in *syn*-**1** compared to *syn*-**5**, which is likely due to energetically favorable thiophene ring overlap offsetting unfavorable steric interactions between them.

Another view of *syn*- and *anti*-**1**, looking through both thiophene-substituted quinoxaline segments, provides additional structural information that is consistent with the fluorescence emission data (Figure 5). A significant degree of π-stacking overlap exists between the quinoxaline rings in both structures, but *syn*-**1** has a higher *overall* degree of overlap compared to *anti*-**1**, given that the thiophene rings are cofacial in the former isomer and not in the latter. Nonetheless, the transannular and centroid-to-centroid distances listed in Table 3 show that the quinoxaline rings are actually closer together in *anti*-**1** compared to *syn*-**1**. Moreover, looking through the aromatic rings, it is apparent that the π-stacking between the quinoxaline rings in *syn*-**1** is slightly askew compared to in *anti*-**1**, resulting in the aromatic segments being slightly slipped (Figure 5). In *anti*-**1**, the centroid-to-centroid distance of 3.810(2) Å and ring offset parameters of 0.492(7) and 0.659(7) Å represent a much closer, direct, face-to-face π-stacking than in *syn*-**1**, with a centroid-to-centroid distance of 4.157(3) Å and ring offset parameters of 0.462(7) and 1.053(8) Å. The latter distortion is likely to be due to slight adjustments being made by a twisting in the aliphatic spacer to allow the thiophene rings in *syn*-**1** to be arranged in an energetically favorable, slightly off-center cofacial stack (Figure 5a, right).[53] Clearly, the structure of *syn*-**1** exhibits a complex interplay between steric strain that pushes the aromatic segments apart and beneficial π-overlap between the thiophene rings that draws them closer together.

As described above, the ^{1}H NMR spectrum of *syn*-**1** suggests restricted rotation about the bond that connects the thiophene and quinoxaline rings, which appears to give rise to two rotamers with respect to the relative orientations of the thiophene rings: eclipsed (sulfur atoms oriented in the same direction) and inverted (sulfur atoms oriented in opposite directions). X-ray crystallographic analysis confirmed that in the solid state there is 2-fold rotational disorder in the thiophene rings of *syn*-**1**, as shown on the left in Figure 5a. Rotation about the thiophene−quinoxaline bond is likely to be restricted because the π-stacked

dx.doi.org/10.1021/jo500053m | J. Org. Chem. 2014, 79, 4312−4321

thiophene rings are too close to rotate past one another, ultimately leading to *syn*-**1** being at least two distinct atropisomeric rotamers in solution and in the solid state, where the eclipsed rotamer is shown on the right in Figure 5a.

CONCLUSION

Synthesis, separation, and characterization of structurally interesting C-shaped diastereomers with cofacially stacked aromatic side arms, *syn*- and *anti*-**1**, has been accomplished. These highly fluorescent molecules showed evidence of ground state $\pi-\pi$ interactions by upfield ^{1}H NMR shifts and red-shifted absorption spectra compared to model compound **2**. They also exhibited large Stokes shifts and a strong positive emission solvatochromism that are indicative of $\pi-\pi$ interactions and charge-transfer character in the excited state, respectively. The X-ray crystal structures of *syn*- and *anti*-**1** revealed a close cofacial arrangement of the thiophene-substituted quinoxaline rings in the solid state. Molecule *syn*-**1** showed evidence of restricted rotation about the bond that connects the thiophene and quinoxaline rings both in solution, based on ^{1}H NMR spectroscopy evidence, and in the solid state, based on rotational disorder observed in the X-ray structure. The subtle but interesting structural differences between the *syn* and *anti* isomers in this study lend themselves naturally to the study of π-stacking behavior because they both have a similar degree of overlap with regard to the quinoxaline rings, but they differ in the relative orientation of attached substituents. As such, we envision that *syn*- and *anti*-**5** could easily be derivatized a myriad of ways using cross-coupling methods to synthesize related structures for further π-stacking studies with the goal of discovering additional interesting, highly emissive materials with different emission color palettes.

EXPERIMENTAL SECTION

General Methods. Conventional reactions were run under inert atmosphere (N_2) using Schlenk line techniques as described. A commercially available monomode CEM Discover microwave unit was used for microwave-assisted reactions, which were run in closed vessels with temperature monitoring in situ using an IR probe. Initially, microwave power was set to 200 W but was modulated automatically by the microwave to reach and maintain the desired temperature. NMR spectroscopy experiments were conducted on 200 and 300 MHz spectrometers, as noted. Chemical shifts (δ) are reported in parts per million (ppm) and are referenced to either TMS (δ = 0.00 ppm for ^{1}H) or residual solvent (δ = 77.23 ppm for ^{13}C). ^{1}H NMR peak multiplicities are reported as s, singlet; d, doublet; t, triplet; m, multiplet; dd, doublet of doublets; and dt, doublet of triplets. Melting points were determined in open capillaries with an electronic apparatus and are uncorrected. $Pd(PPh_3)_4$ was purchased from Strem Chemicals, Inc. All other solvents and chemicals were reagent-grade, purchased from commercial sources and used without further purification, unless otherwise noted. Chloroform used in the synthesis of **4** was washed twice with deionized H_2O, dried over anhydrous $CaCl_2$, and distilled over P_2O_5. Analytical and preparative thin layer chromatography separations were performed on EMD TLC silica gel 60 F_{254} plates and on EMD 1.0 mm silica gel 60 F_{254} plates, respectively. Flash chromatography was performed using EMD silica gel 60 (230−400 mesh ASTM). UV−vis and fluorescence spectroscopy measurements were carried out in 1 cm path length quartz cuvettes at room temperature. High-resolution mass spectra (HRMS) were determined on a QTOF spectrometer.

(1α,2β,4β,5α,8α,9β,11β,12α)-1,5,6,7,8,12,13,14-Octachloro-15,15,16,16-tetramethoxypentacyclo[10.2.1.1^{5,8}.0^{2,11}.0^{4,9}]-hexadeca-6,13-diene (3). A 10 mL microwave vessel equipped for magnetic stirring was charged with 1.5 mL (8.52 mmol) of 1,2,3,4-tetrachloro-5,5-dimethoxycyclopentadiene, 0.390 mL (4.12 mmol) of 1,4-cyclohexadiene, and 1.4 mL of *p*-xylene. The vessel was capped and heated to 200 °C with stirring for 30 min in a CEM microwave. The resulting reaction mixture was washed with hexanes (3 mL), and **3** was isolated in vacuo as a white crystalline solid that required no further purification in 70% yield (1.76 g). Compound **3** (mp 249−252 °C w/ prior softening; lit.[33] 250−252 °C): ^{1}H NMR (200 MHz, $CDCl_3$) δ 3.58 (s, 6H), 3.54 (s, 6H), 2.63−2.48 (m, 4H), 1.90 (dt, J = 13, 4.3 Hz, 2H), 0.64−0.44 (m, 2H); ^{13}C NMR (50 MHz, $CDCl_3$) δ 129.7, 112.4, 78.5, 52.9, 51.8, 45.6, 18.7.

Synthesis and Separation of *syn*- and *anti*-5. Compound **3** (600 mg, 0.987 mmol) was oxidized following a previously reported procedure[6] to give bis-α-diketone **4** in 80% yield (417 mg) as a bright yellow solid. Compound **4**: ^{1}H NMR (200 MHz, 50:50 DMSO-d_6/$CDCl_3$) δ 3.71 (s, 6H), 3.51 (s, 6H), 3.04−2.90 (m, 4H), 1.84−1.77 (m, 2H), 0.40−0.22 (m, 2H). A 10 mL microwave vessel equipped for magnetic stirring was charged with 100 mg (0.189 mmol) of **4**, 5 mg (0.028 mmol) of $Zn(OAc)_2$, and 159 mg (0.851 mmol) of 4-bromo-1,2-diaminobenzene. A 2 mL portion of chlorobenzene was added to the vessel via syringe. The mixture was stirred briefly prior to purging the headspace with nitrogen. The vessel was capped and heated to 200 °C with stirring for 30 min in a CEM microwave. Upon completion, the dark brown suspension was filtered through a cotton plug to afford a brown solution. The solvent was removed by evaporation, and the crude mixture was purified by column chromatography (eluent, 20% ethyl acetate in hexanes; R_f of *syn*-**5**, 0.16; R_f of *anti*-**5**, 0.22). The resulting sample of *syn*-**5** required a second purification by column chromatography.

(1α,2β,4β,5α,16α,17β,19β,20α)-7,14,22,29-Tetraaza-10,26-dibromo-1,5,16,20-tetrachloro-31,31,32,32-tetramethoxynonacyclo-[18.10.1.1^{5,16}.0^{2,19}.0^{4,17}.0^{6,15}.0^{8,13}.0^{21,30}.0^{23,28}]dotriaconta-6-(15),7,9,11,13,21(30),22,24,26,28-decaene (*syn*-5). Off-white crystalline solid (31 mg; 20%). *syn*-**5** (mp >300 °C dec): ^{1}H NMR (200 MHz, $CDCl_3$) δ 7.99 (d, J = 2.0 Hz, 2H), 7.68 (d, J = 8.9, 2.0 Hz, 2H), 7.59 (d, J = 8.8 Hz, 2H), 3.73 (s, 6H), 3.33 (s, 6H), 2.97−2.80 (m, 4H), 2.02−1.90 (m, 2H), −1.18 (m, 2H); ^{13}C NMR (75 MHz, $CDCl_3$) δ 153.1, 152.5, 141.9, 140.2, 133.3, 131.2, 130.0, 124.3, 111.4, 74.9, 74.8, 52.6, 52.2, 43.4, 43.1, 19.82, 19.77. HRMS-ESI (m/z): $[M + H]^+$ calcd for $C_{32}H_{27}Br_2Cl_4N_4O_4$, 828.9153; found, 828.9144.

(1α,2β,4β,5α,16α,17β,19β,20α)-7,14,22,29-Tetraaza-11,26-dibromo-1,5,16,20-tetrachloro-31,31,32,32-tetramethoxynonacyclo-[18.10.1.1^{5,16}.0^{2,19}.0^{4,17}.0^{6,15}.0^{8,13}.0^{21,30}.0^{23,28}]dotriaconta-6-(15),7,9,11,13,21(30),22,24,26,28-decaene (*anti*-5). Off-white crystalline solid (48 mg; 31%). *anti*-**5** (mp >300 °C dec): ^{1}H NMR (200 MHz, $CDCl_3$) δ 7.94 (d, J = 2.2 Hz, 2H), 7.79 (dd, J = 9.0, 2.2 Hz, 2H), 7.63 (d, J = 8.8 Hz, 2H), 3.73 (s, 6H), 3.34 (s, 6H), 2.91−2.85 (m, 4H), 2.02−1.94 (m, 2H), −1.22 (m, 2H); ^{13}C NMR (50 MHz, $CDCl_3$) δ 153.0, 152.5, 141.8, 140.1, 133.2, 131.4, 130.0, 124.1, 111.4, 74.94, 74.89, 52.5, 52.2, 43.2, 43.1, 19.8. HRMS-ESI (m/z): $[M + H]^+$ calcd for $C_{32}H_{27}Br_2Cl_4N_4O_4$, 828.9153; found, 828.9144.

(1α,2β,4β,5α,16α,17β,19β,20α)-7,14,22,29-Tetraaza-1,5,16,20-tetrachloro-31,31,32,32-tetramethoxy-10,26-di(2-thienyl)-nonacyclo[18.10.1.1^{5,16}.0^{2,19}.0^{4,17}.0^{6,15}.0^{8,13}.0^{21,30}.0^{23,28}]-dotriaconta-6(15),7,9,11,13,21(30),22,24,26,28-decaene (*syn*-1). A 10 mL microwave vessel equipped with a stir bar was charged with 40 mg (0.048 mmol) of *syn*-**5** and 24 mg (0.19 mmol) of 2-thienylboronic acid, followed by 2 mL of toluene and 0.5 mL of absolute ethanol. Nitrogen gas (N_2) was bubbled through the mixture. A 0.17 mL portion of an aqueous Na_2CO_3 solution (0.2 g/mL) was added, followed by 10 mg (0.009 mmol) of $Pd(PPh_3)_4$. The headspace was purged with N_2. The vessel was heated to 120 °C for 30 min with stirring in a CEM microwave. Upon completion, the contents were transferred to a separatory funnel, and the biphasic reaction mixture was extracted with ethyl acetate. The combined organic extracts were washed once with water and once with brine. The organic layer was dried over anhydrous $MgSO_4$, and the solvent was removed in vacuo. The crude product was purified via chromatography on silica gel with 40% ethyl acetate in hexanes as the eluent to give *syn*-**1** as a yellow solid (21 mg; 53% yield). *syn*-**1** (mp >300 °C dec): ^{1}H NMR (200 MHz, $CDCl_3$) δ 7.95−7.94 (m, 2H), 7.76−7.65 (m, 4H), 7.16 (dd, J = 5.1, 1.1 Hz, 2H), 7.11 (dd, J = 3.6, 1.2 Hz, 2H), 6.85 (dd, J = 5.0, 3.8 Hz, 2H), 3.74 (s, 6H), 3.35 (s, 6H), 3.00−2.81 (m, 4H), 2.09−1.95 (m, 2H), −1.01 (m, 2H); ^{13}C NMR (75 MHz, $CDCl_3$) δ 152.7, 151.5, 142.4, 141.8, 140.8, 135.8, 129.2, 128.6,

dx.doi.org/10.1021/jo500053m | J. Org. Chem. 2014, 79, 4312−4321

127.6, 126.5, 124.6, 123.9, 111.4, 75.04, 74.99, 52.5, 52.2, 43.6, 43.3, 19.85, 19.80. HRMS-ESI (m/z): $[M + H]^+$ calcd for $C_{40}H_{33}Cl_4N_4O_4S_2$, 837.0697; found, 837.0705.

(1α,2β,4β,5α,16α,17β,19β,20α)-7,14,22,29-Tetraaza-1,5,16,20-tetrachloro-31,31,32,32-tetramethoxy-11,26-di(2-thienyl)-nonacyclo[18.10.1.1^{5,16}.0^{2,19}.0^{4,17}.0^{6,15}.0^{8,13}.0^{21,30}.0^{23,28}]-dotriaconta-6(15),7,9,11,13,21(30),22,24,26,28-decaene (*anti*-1). A 10 mL microwave vessel equipped with a stir bar was charged with 51 mg (0.061 mmol) of *anti*-**5**, followed by 2.4 mL of toluene and 0.6 mL of absolute ethanol. Nitrogen gas (N_2) was bubbled through the mixture. A 31 mg (0.24 mmol) portion of 2-thienylboronic acid was added, followed by 10 mg (0.009 mmol) of $Pd(PPh_3)_4$. A 0.21 mL portion of an aqueous Na_2CO_3 solution (0.2 g/mL) was added, and the headspace was purged with N_2. The vessel was heated to 120 °C for 30 min with stirring in a CEM microwave. Upon completion, the contents were transferred to a separatory funnel, and the biphasic reaction mixture was extracted with ethyl acetate. The combined organic extracts were washed once with water and once with brine. The organic layer was dried over anhydrous $MgSO_4$, and the solvent was removed in vacuo. The crude compound was purified by chromatography on silica gel using 30% ethyl acetate in hexanes, followed by additional purification with 40% ethyl acetate in hexanes on silica gel to give *anti*-**1** as a yellow solid (33 mg; 65% yield). *anti*-**1** (mp >300 °C dec): ^{1}H NMR (200 MHz, $CDCl_3$) δ 7.98 (d, J = 1.8 Hz, 2H), 7.64 (d, J = 8.6 Hz, 2H), 7.46 (dd, J = 5.0, 1.2 Hz, 2H), 7.37 (dd, J = 8.8, 2.0 Hz, 2H), 7.23 (dd, J = 3.6, 1.2 Hz, 2H), 7.17 (dd, J = 5.0, 3.8 Hz, 2H), 3.74 (s, 6H), 3.36 (s, 6H), 2.98−2.80 (m, 4H), 2.05−1.98 (m, 2H), −1.06 (m, 2H); ^{13}C NMR (75 MHz, $CDCl_3$) δ 152.6, 151.6, 142.8, 141.8, 140.8, 135.7, 129.0, 128.6, 127.6, 127.0, 125.0, 124.2, 111.4, 75.05, 75.02, 52.5, 52.2, 43.35, 43.32, 19.8. HRMS-ESI (m/z): $[M + H]^+$ calcd for $C_{40}H_{33}Cl_4N_4O_4S_2$, 837.0697; found, 837.0694.

5,12-Diaza-9-bromo-1,2,2-trimethyltetracyclo[10.2.1.0^{4,13}.0^{6,11}]-pentadeca-4(13),5,7,9,11-pentaene and 5,12-Diaza-8-bromo-1,2,2-trimethyltetracyclo[10.2.1.0^{4,13}.0^{6,11}]pentadeca-4-(13),5,7,9,11-pentaene (7). A 25 mL, two-neck round-bottom flask containing a stir bar was charged with 166 mg (1.0 mmol) of (±)-camphorquinone (**6**), 187 mg (1.0 mmol) of 4-bromo-1,2-diaminobenzene, and 3 mL of ethanol. The resulting solution was stirred until the solids dissolved. A 25 mg (0.10 mmol) portion of $CuSO_4{\cdot}5H_2O$ was added, and the reaction mixture was stirred at room temperature for 100 min. The reaction mixture was filtered, and the solvent was removed by evaporation. The crude product was purified by column chromatography on silica gel (eluent: 100% CH_2Cl_2) to give **7** as a mixture of regioisomers in the form of a white solid (141 mg; 44% yield). Compound **7** (when applicable, separate peaks arising from each regioisomer are listed in pairs): ^{1}H NMR (200 MHz, $CDCl_3$) δ 8.21 and 8.14 ppm (2d, J = 2.2, 2.2 Hz, 1H), 7.89 and 7.84 (2d, J = 9.2, 8.8 Hz, respectively, 1H), 7.74−7.68 (m, 1H), 3.07 and 3.04 (2s, 1H), 2.42−1.98 (m, 2H), 1.48−1.32 (m, 5H), 1.12 (s, 3 H), 0.61 (s, 3H); ^{13}C NMR (50 MHz, $CDCl_3$) δ 166.5 (and 166.0), 164.7 (and 164.2), 142.4 (and 142.3), 140.5 (and 140.3), 131.5, 131.4 (and 131.3), 130.2 (and 130.1), 121.7, 54.3, 54.0, 53.4, 31.9, 24.6, 20.4, 18.6, 10.1. HRMS-ESI (m/z): $[M + H]^+$ calcd for $C_{16}H_{18}BrN_2$, 317.0653; found, 317.0648.

5,12-Diaza-1,2,2-trimethyl-9-(2-thienyl)tetracyclo[10.2.1.0^{4,13}.0^{6,11}]-pentadeca-4(13),5,7,9,11-pentaene and 5,12-Diaza-1,2,2-trimethyl-8-(2-thienyl)tetracyclo[10.2.1.0^{4,13}.0^{6,11}]pentadeca-4(13),5,7,9,11-pentaene (2). A 10 mL microwave vessel equipped with a stir bar was charged with 50 mg (0.158 mmol) of compound **7** and 40 mg (0.316 mmol) of 2-thienylboronic acid, followed by 4 mL of toluene and 1 mL of absolute ethanol. The vessel was capped, and the solution was purged with N_2 gas. A 0.17 mL portion of an aqueous Na_2CO_3 solution (0.2 g/mL) was added, followed by 20 mg (0.0158 mmol) of $Pd(PPh_3)_4$. The headspace was purged with N_2. The vessel was heated to 120 °C with stirring for 30 min in a CEM microwave. The reaction mixture was transferred to a separatory funnel, and the aqueous layer was extracted twice with ethyl acetate. The organic extracts were combined and washed once with deionized water and once with brine. The organic layer was dried over anhydrous $MgSO_4$, and the solvent was removed in vacuo. The crude product was purified via chromatography on silica gel (eluent: 20% ethyl acetate in hexanes) followed by recrystallization from 20% ethyl acetate in hexanes to give **2** as a mixture of regioisomers in the form of a colorless crystalline solid (6 mg; 12% yield). Compound **2** (when applicable, separate peaks arising from each regioisomer are listed in pairs): ^{1}H NMR (200 MHz, $CDCl_3$) δ 8.28 and 8.22 (2d, J = 2.0, 2.0 Hz, 1H), 8.05−7.88 (m, 2H), 7.49 (dd, J = 3.6, 1.2 Hz, 1H), 7.35 (dd, J = 5.1, 1.2 Hz, 1H), 7.13 (dd, J = 5.2, 3.6 Hz, 1H), 3.07 and 3.05 (2s, 1H), 2.42−1.97 (m, 2H), 1.50−1.36 (m, 5H), 1.13 (s, 3H), 0.65 (s, 3H); ^{13}C NMR (50 MHz, $CDCl_3$) δ 166.4 (and 165.6), 164.6 (and 163.8), 143.7, 142.0 (and 141.8), 141.2 (and 140.9), 134.4, 129.4 (and 129.3), 128.5, 126.4, 126.0, 125.1 (and 125.0), 124.3, 54.4, 54.0, 53.5, 32.1, 24.8, 20.5, 18.7, 10.2. HRMS-ESI (m/z): $[M + H]^+$ calcd for $C_{20}H_{21}N_2S$, 321.1425; found, 321.1412.

Crystallographic Data Collection and Refinement. X-ray crystallography was performed using a CCD platform diffractometer (Mo Kα (λ = 0.71073 Å)) at 125 K. The crystals were selected under a microscope and mounted in a nylon loop with cryoprotectant oil. The structures were solved using direct methods and standard difference map techniques and were refined by full-matrix least-squares procedures on F^2 with SHELXTL (v2008).[54] All non-hydrogen atoms were refined anisotropically. Hydrogen atoms on carbon were included in calculated positions and were refined using a riding model. The structure of *syn*-**5** contained a disordered hexane solvate, which was treated as a diffuse contribution to the overall scattering without specific atom positions with SQUEEZE/PLATON.[55] The structure of *anti*-**1** was found to be nonmerohedrally twinned. The two-component orientation matrix produced by CELL_NOW was used to integrate the data, which was subsequently scaled and absorption corrected with TWINABS (v2008/4).[54] The initial solution was refined with single-component data for the stronger domain before final refinement with data from both domains.

■ ASSOCIATED CONTENT

Ⓢ Supporting Information

^{1}H and ^{13}C NMR spectra, UV−vis spectra, crystallographic data, and CIF files. This material is available free of charge via the Internet at http://pubs.acs.org.

■ AUTHOR INFORMATION

Corresponding Author

*E-mail: jocelyn.nadeau@marist.edu.

Notes

The authors declare no competing financial interest.

■ ACKNOWLEDGMENTS

J.M.N. wishes to recognize the donors of the American Chemical Society Petroleum Research Fund and Marist College for funding and to acknowledge Dr. Teresa A. Garrett and Karen Wovkulich from Vassar College for their assistance with the exact mass spectrometry (National Science Foundation Grant No. 1039659 to T.A.G.) and the 300 MHz NMR spectroscopy experiments, respectively. J.M.T. acknowledges the National Science Foundation for supporting the X-ray diffraction facility at Vassar College (Grant Nos. 0521237 and 0911324 to J.M.T.).

■ REFERENCES

(1) For example, see Forrest, S. R.; Thompson, M. E. *Chem. Rev.* **2007**, *107* (4), 923−925.

(2) Tour, J. M. *Molecular Electronics: Commercial Insights, Chemistry, Devices, Architecture and Programming*; World Scientific: River Edge, NJ, 2003.

(3) Brédas, J.; Belijonne, D.; Coropceanu, V.; Cornil, J. *Chem. Rev.* **2004**, *104*, 4971−5003.

(4) Roncali, J. *Chem. Rev.* **1992**, *92*, 711−738.

(5) *Handbook of Conducting Polymers*, 3rd ed.; Skotheim, T. A., Reynolds, J. R., Eds.; CRC: Boca Raton, FL, 2007.
(6) Chou, T.-C.; Liao, K.-C.; Lin, J.-J. *Org. Lett.* **2005**, *7*, 4843−4846.
(7) Chou, T.-C.; Lin, K.-C.; Wu, C.-A. *Tetrahedron* **2009**, *65*, 10243−10257.
(8) Etzkorn, M.; Timmerman, J. C.; Brooker, M. D.; Yu, X.; Gerken, M. *Beilstein J. Org. Chem.* **2010**, No. 39.
(9) Klärner, F.-G.; Kahlert, B. *Acc. Chem. Res.* **2003**, *36*, 919−932.
(10) Nadeau, J. M.; Liu, M.; Waldeck, D. H.; Zimmt, M. B. *J. Am. Chem. Soc.* **2003**, *125*, 15964−15973.
(11) DeBlase, A. F.; Thong, D. C.; Nadeau, J. M.; Gebhart, D.; Provo, J.; Foxman, B. M. *Acta Crystallogr.* **2009**, *E65*, o2427−o2428.
(12) Nemoto, H.; Kawano, T.; Ueji, N.; Bando, M.; Kido, M.; Suzuki, I.; Shibuya, M. *Org. Lett.* **2000**, *2*, 1015−1017.
(13) Chou, T.-C.; Hwa, C.-L.; Lin, J.-J.; Liao, K.-C.; Tseng, J.-C. *J. Org. Chem.* **2005**, *70*, 9717−9726.
(14) Chou, T.-C.; Liao, K.-C.; Hwa, C.-L.; Tseng, J.-C. *J. Chin. Chem. Soc.* **2012**, *59*, 345−356.
(15) Thirion, D.; Poriel, C.; Barrière, F.; Métivier, R.; Jeannin, O.; Rault-Berthelot, J. *Org. Lett.* **2009**, *11*, 4794−4797.
(16) Coropceanu, V.; Cornil, J.; da Silva Filho, D. A.; Olivier, Y.; Sibley, R.; Brédas, J.-L. *Chem. Rev.* **2007**, *107*, 926−952.
(17) Bartholomew, G. P.; Bazan, G. C. *Acc. Chem. Res.* **2001**, *34*, 30−39.
(18) Salhi, F.; Collard, D. M. *Adv. Mater.* **2003**, *15*, 81−85.
(19) Schneebeli, S. T.; Kamenetska, M.; Cheng, Z.; Skouta, R.; Friesner, R. A.; Venkataraman, L.; Breslow, R. *J. Am. Chem. Soc.* **2011**, *133*, 2136−2139.
(20) Morisaki, Y.; Sawamura, T.; Murakami, T.; Chujo, Y. *Org. Lett.* **2010**, *12*, 3188−3191.
(21) Yoo, H.; Yang, J.; Yousef, A.; Wasielewski, M. R.; Kim, D. *J. Am. Chem. Soc.* **2010**, *132*, 3939−3944.
(22) Jagtap, S. P.; Collard, D. M. *J. Am. Chem. Soc.* **2010**, *132*, 12208−12209.
(23) Jagtap, S. P.; Mukhopadhyay, S.; Coropceanu, V.; Brizius, G. L.; Brédas, J.-L.; Collard, D. M. *J. Am. Chem. Soc.* **2012**, *134*, 7176−7185.
(24) Knoblock, K. M.; Silvestri, C. J.; Collard, D. M. *J. Am. Chem. Soc.* **2006**, *128*, 13680−13681.
(25) Kaikawa, T.; Takimiya, K.; Aso, Y.; Otsubo, T. *Org. Lett.* **2000**, *2*, 4197−4199.
(26) Iyoda, M.; Kondo, T.; Nakao, K.; Hara, K.; Kuwatani, Y.; Yoshida, M.; Matsuyama, H. *Org. Lett.* **2000**, *2*, 2081−2083.
(27) Takita, R.; Song, C.; Swager, T. M. *Org. Lett.* **2008**, *10*, 5003−5005.
(28) Rathore, R.; Abdelwahed, S. H.; Guzei, I. A. *J. Am. Chem. Soc.* **2003**, *125*, 8712−8713.
(29) Yamamoto, T.; Zhou, Z.-h.; Kanbara, T.; Shimura, M.; Kizu, K.; Maruyama, T.; Nakamura, Y.; Fukuda, T.; Lee, B.-L.; Ooba, N.; Tomaru, S.; Kurihara, T.; Kaino, T.; Kubota, K.; Sasaki, S. *J. Am. Chem. Soc.* **1996**, *118*, 10389−10399.
(30) Choi, Y.-S.; Lee, W.-h.; Kim, J.-R.; Lee, S.-K.; Shin, W.-S.; Moon, S.-J.; Park, J.-W.; Kang, I.-N. *Bull. Korean Chem. Soc.* **2011**, *32*, 417−423.
(31) Lindgren, L. J.; Zhang, F.; Andersson, M.; Barrau, S.; Hellström, S.; Mammo, W.; Perzon, E.; Inganäs, O.; Andersson, M. R. *Chem. Mater.* **2009**, *21*, 3491−3502.
(32) Wang, E.; Hou, L.; Wang, Z.; Ma, Z.; Hellström, S.; Zhuang, W.; Zhang, F.; Inganäs, O.; Andersson, M. R. *Macromolecules* **2011**, *44*, 2067−2073.
(33) Chou, T.-C.; Yang, M.-S.; Lin, C.-T. *J. Org. Chem.* **1994**, *59*, 661−663.
(34) Khan, F. A.; Prabhudas, B.; Dash, J.; Sahu, N. *J. Am. Chem. Soc.* **2000**, *122*, 9558−9559.
(35) Khan, F. A.; Dash, J. *J. Am. Chem. Soc.* **2002**, *124*, 2424−2425.
(36) Heravi, M. M.; Taheri, S.; Bakhtiari, K.; Oskooie, H. A. *Catal. Commun.* **2007**, *8*, 211−214.
(37) Thirion, D.; Poriel, C.; Métivier, R.; Rault-Berthelot, J.; Barrière, F.; Jeannin, O. *Chem.—Eur. J.* **2011**, *17*, 10272−10287.
(38) Reichardt, C.; Welton, T. *Solvents and Solvent Effects in Organic Chemistry*, 4th ed.; Wiley-VCH: Weinheim, Germany, 2011.
(39) Thirion, D.; Romain, M.; Rault-Berthelot, J.; Poriel, C. *J. Mater. Chem.* **2012**, *22*, 7149−7157.
(40) Boens, N.; Qin, W.; Basarić, N.; Hofkens, J.; Ameloot, M.; Pouget, J.; Lefèvre, J.-P.; Valeur, B.; Gratton, E.; vandeVen, M.; Silva, N. D., Jr.; Engelborghs, Y.; Willaert, K.; Sillen, A.; Rumbles, G.; Phillips, D.; Visser, A. J. W. G.; van Hoek, A.; Lakowicz, J. R.; Malak, H.; Gryczynski, I.; Szabo, A. G.; Krajcarski, D. T.; Tamai, N.; Miura, A. *Anal. Chem.* **2007**, *79*, 2137−2149.
(41) Fery-Forgues, S.; Lavabre, D. *J. Chem. Educ.* **1999**, *76*, 1260−1264.
(42) Lakowicz, J. R. *Principles of Fluorescence Spectroscopy*, 3rd Ed.; Springer: New York, 2006.
(43) Chen, S.; Xu, X.; Liu, Y.; Qiu, W.; Yu, G.; Wang, H.; Zhu, D. *J. Phys. Chem. C* **2007**, *111*, 1029−1034.
(44) Bhattacharyya, K.; Chowdhury, M. *Chem. Rev.* **1993**, *93*, 507−535.
(45) Turro, N. J. *Modern Molecular Photochemistry*; University Science Books: Mill Valley, CA, 1991.
(46) Pedireddi, V. R.; Reddy, D. S.; Goud, B. S.; Craig, D. C.; Rae, A. D.; Desiraju, G. R. *J. Chem. Soc., Perkin Trans. 2* **1994**, 2353−2360.
(47) Lueckheide, M.; Rothman, N.; Ko, B.; Tanski, J. M. *Polyhedron* **2013**, *58*, 79−84.
(48) Macrae, C. F.; Edgington, P. R.; McCabe, P.; Pidcock, E.; Shields, G. P.; Taylor, R.; Towler, M.; van de Streek, J. *J. Appl. Crystallogr.* **2006**, *39*, 453−457.
(49) Calculated with Olex2: Dolomanov, O. V.; Bourhis, L. J.; Gildea, R. J.; Howard, J. A. K.; Puschmann, H. *J. Appl. Crystallogr.* **2009**, *42*, 339−341.
(50) Hargreaves, A.; Rizvi, S. H. *Acta Crystallogr.* **1962**, *15*, 365−373.
(51) Almenningen, A.; Bastiansen, O.; Fernholt, L.; Cyvin, B. N.; Cyvin, S. J.; Samdal, S. *J. Mol. Struct.* **1985**, *128*, 59−76.
(52) Johansson, M. P.; Olsen, J. *J. Chem. Theory Comput.* **2008**, *4*, 1460−1471.
(53) Martinez, C. R.; Iverson, B. L. *Chem. Sci.* **2012**, *3*, 2191−2201.
(54) Sheldrick, G. M. *Acta Crystallogr.* **2008**, *A64*, 112−122.
(55) Spek, A. L. *Acta Crystallogr.* **2009**, *D65*, 148−155.